A virtual wind tunnel for deforming airborne wind energy kites

Poland, Jelle Agatho Wilhelm ; Schmehl, Roland

DOI
10.1088/1742-6596/2767/7/072001

Publication date
2024

Document Version
Final published version

Published in
Journal of Physics: Conference Series

A virtual wind tunnel for deforming airborne wind energy kites

Journal of Physics: Conference Series **2767** (2024) 072001 doi:10.1088/1742-6596/2767/7/072001

A virtual wind tunnel for deforming airborne wind energy kites

Jelle Agatho Wilhelm Poland, Roland Schmehl

Faculty of Aerospace Engineering, Delft University of Technology, Kluyverweg 1, 2629 HS, Delft

E-mail: J.A.W.Poland@tudelft.nl

Abstract. This paper presents a quasi-steady simulation framework for soft-wing kites with suspended control unit employed for airborne wind energy. The kites are subject to actuation-induced and aero-elastic deformation and are described by a coupled aero-structural model in a virtual wind tunnel setup. Key contributions of the present work are a kinetic dynamic relaxation algorithm and a procedure to define a physically consistent initial state. For symmetric actuation, the kite is pitch-statically stable and the simulations converge to a static equilibrium state. Most soft-wing kites are not roll-statically stable and do not find a static equilibrium without a symmetry assumption, as this introduces non-zero roll- and yaw moments. Another important contribution is the introduction of a steady circular flight state that enables convergence without a symmetry assumption. By neglecting gravity, the kite can fly in a perfectly circular turning motion around the wind vector with a constant radius and constant rotational velocity without requiring active control input. In an idealized wind-aligned tether case, the difference in aerodynamic- and centrifugal force application centers makes it impossible to achieve both a force- and moment equilibrium. This was resolved by including an elevation angle that introduces a radial tether force component, which introduces a centrifugal and aerodynamic force difference. Therefore, an operating point with roll equilibrium can be found where the kite finds a static equilibrium, enabling the first quasi-steady simulations of turning flights. Simulated quantifications of soft-wing kite turning behavior, i.e., turning laws, contribute to better kite- and control design.

1. Introduction

Airborne wind energy (AWE) systems deploy tethered flying devices to harvest wind energy. The technology promises to use up to 90% less material than conventional wind turbines [1], resulting in a lower environmental footprint, potentially lower costs, and access thus far untapped wind resources at higher altitudes [2]. From the numerous concepts, this study is focused on the soft-wing AWE systems that use the pulling force of a kite maneuvered in cross-wind patterns to drive a ground-based drum generator; see Figure 1(a). Due to a finite tether length, there is a reel-out and a reel-in phase. Because the reel-in phases are shorter and the pulling force is lower, net energy is generated. The cyclic operation is called the pumping cycle and consists of a reel-in, transition, and reel-out phase.

The present study is based on the TU Delft V3 kite illustrated in Figure 1, comprising a leading-edge inflatable (LEI) wing, a bridle line system, and an autonomous cable robot known as the kite control unit (KCU). The wing is actuated as a morphing aerodynamic control surface and is subject to strong aero-structural coupling. The wing consists of an inflated tubular

frame, combining a leading edge (LE) tube and several connected strut tubes, to which a fabric membrane, denoted as the canopy, is attached. The depower tape is used for symmetrically actuating the rear bridle lines, modifying the pitch of the wing relative to the KCU and, through that, the angle relative to the inflow and, consequently, the aerodynamic loading. The steering tape is used for asymmetrically actuating the rear bridle lines, pulling in one half of the trailing edge while releasing the other. This causes the wing to yaw, roll, and asymmetrically deform by twisting along the span, creating an aerodynamic side force leading to a turning maneuver [3].

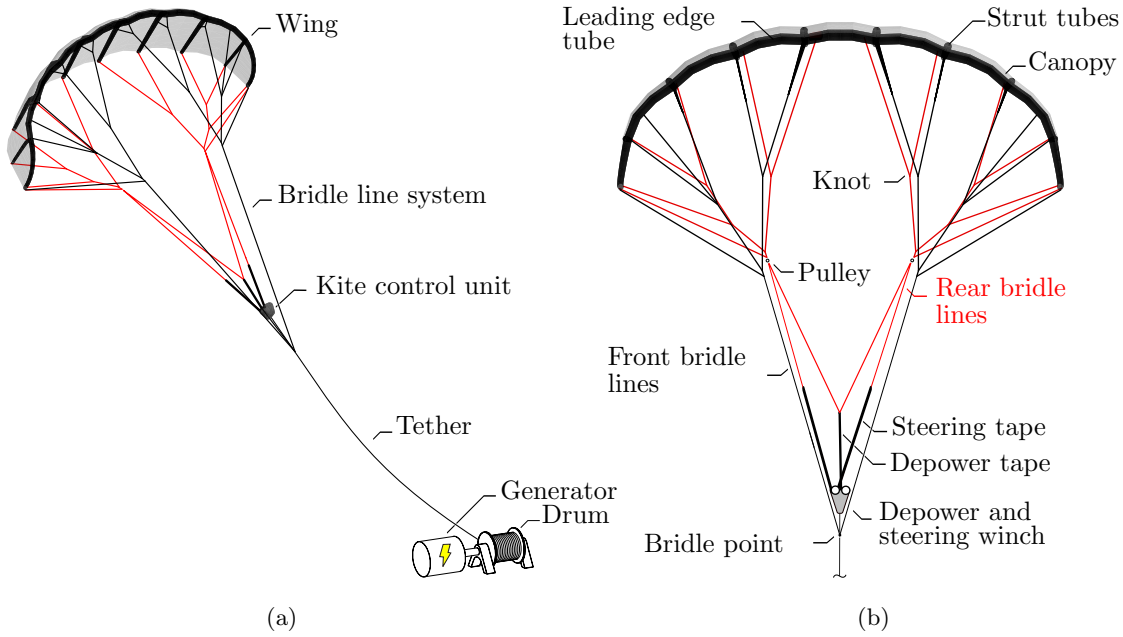

Figure 1: Soft-wing ground-generating AWE system [4]. (**a**) Complete AWE system. (**b**) Kite front view. The original TU Delft V3 kite is depicted, which was further developed by Kitepower B.V. [5]. The front bridle lines attached to the LE are colored black, while the rear bridle lines attached to the trailing edge (TE) are colored red.

Assessing the performance and flight characteristics of 25-500m2 AWE soft-wing kites can be done through flight tests. These are expensive and, without knowing the dynamic behavior upfront, come with elevated risks. Wind tunnels would pose a safer alternative, but at current sizes, they require a scaled-down kite. Because the aerodynamic and structural forces don't scale at the same rate, the aero-elastic effects of a perfectly scaled-down kite will differ, leaving a wind tunnel test unrepresentative. The alternative is a purely simulation-based approach, where the environment is defined as a virtual wind tunnel (VWT), where one can focus on the kite design alone [6]. Focusing on the kite aids in solving the challenges arising from modeling soft-wing kites with a curved wing shape, subject to actuation-induced morphing and strong aero-structural coupling. The VWT simulates discrete operating points that combined make up the flight path, each having reached a quasi-steady equilibrium state. This is possible because a reduced order frequency analysis shows that it can be assumed that the kite transitions through a sequence of quasi-steady flight and deformation states while advancing along the flight trajectory [6].

A VWT quasi-steady aero-structural coupled simulation requires an equilibrium over all six degrees of freedom (DOF) to converge. Due to the inherent instability of most soft-wing kite systems, continuous control input is required. To avoid needing active control within the simulation, VWT implementations [4,6] simulate an operating point that, without asymmetrical

disturbances, finds an equilibrium. This limits the analysis to operating points where a symmetry assumption holds, e.g., straight symmetric flight parallel to the wind.

Thedens [6] applied the VWT concept to a ram-air kite, using a staggered coupling scheme to combine a structural finite element solver with dynamic relaxation and a potential flow solver, which proved numerically stable for determining the wing's equilibrium shape under aerodynamic load. Poland and Schmehl [4] placed the V3 LEI kite in a VWT environment, forming the basis of this paper.

The presented novel approach enables simulations without a symmetry assumption, using a steady circular turning flight state. To the author's knowledge, these are the first quasi-steady turning flight simulations enabling quantification of soft-wing kite turning abilities, often expressed in a simplified turning-rate law [7], without the need for empirical input. Besides aiding kite design, a non-empirically based turning-rate law allows one to perform control design and gain-tuning before flight.

The remainder of this paper is organized as follows. In Section 2, the pursued method is described. Section 3 explains the VWT simulation setup in symmetric and steady circular flight. In Section 4, the results are presented. In Section 5, conclusions are drawn, and recommendations for future work are provided.

2. Method Revisited

Poland and Schmehl [4] used a particle system model (PSM) to describe the aero-structural behavior of the kite, as illustrated in Figure 2(a). Cayon et al. [8] continued this work and added a Vortex-Step Method (VSM) as depicted in Figure 2(b) coupled to 2D precomputed Reynolds-Averaged Navier Stokes Computational Fluid Dynamic simulations from Breukels [3]. A fast aero-structural coupled model is selected to develop a robust engineering design model. The simulation framework is based on these studies, with the following improvements.

The uniform mass distribution over the kite has been replaced by computing each nodal mass based on the attached elements.

Aerodynamic bridle line forces are modeled as inclined cylinders, neglecting vibration-induced loads and using empirical relations for the lift- and drag coefficients [9],

$$C_{\mathrm{L,cylinder}} = C_{\mathrm{L}} \sin^2 \Theta \cos \Theta, \tag{1}$$

$$C_{\mathrm{D,cylinder}} = C_{\tau} \sin^3 \Theta + C_{\mathrm{f}}, \tag{2}$$

where Θ represents the angle between the bridle line and apparent wind speed, C_{τ} the normal drag coefficient and C_{f} the shear drag coefficient [6]. For the node representing the KCU, an additional drag contribution is calculated. Assuming the shape represents an extrusion of an isosceles triangle [10], a volume is calculated and used to compute a representative equivalent sphere diameter (D_{eq}),

$$D_{\mathrm{eq}} = \sqrt[3]{\frac{3\,whl}{\pi}}, \tag{3}$$

where w represents the width of the isoscele, h the height and l the length. With an equivalent sphere diameter, a Reynolds Number is calculated and used to find the drag coefficient of the KCU through empirical sphere drag relations [9].

The functional-programmed solver architecture [4] has been replaced by an object-oriented programming framework [11] that feeds one-dimensional vectors to an implicit Euler integration scheme using a BiConjugate Gradient Stabilized Method algorithm [12] as the iterative solver. Finding the quasi-steady shape of the kite falls under the class of form-finding problems, of which a dynamic relaxation technique called kinetic dynamic relaxation (KDR) [13] was selected

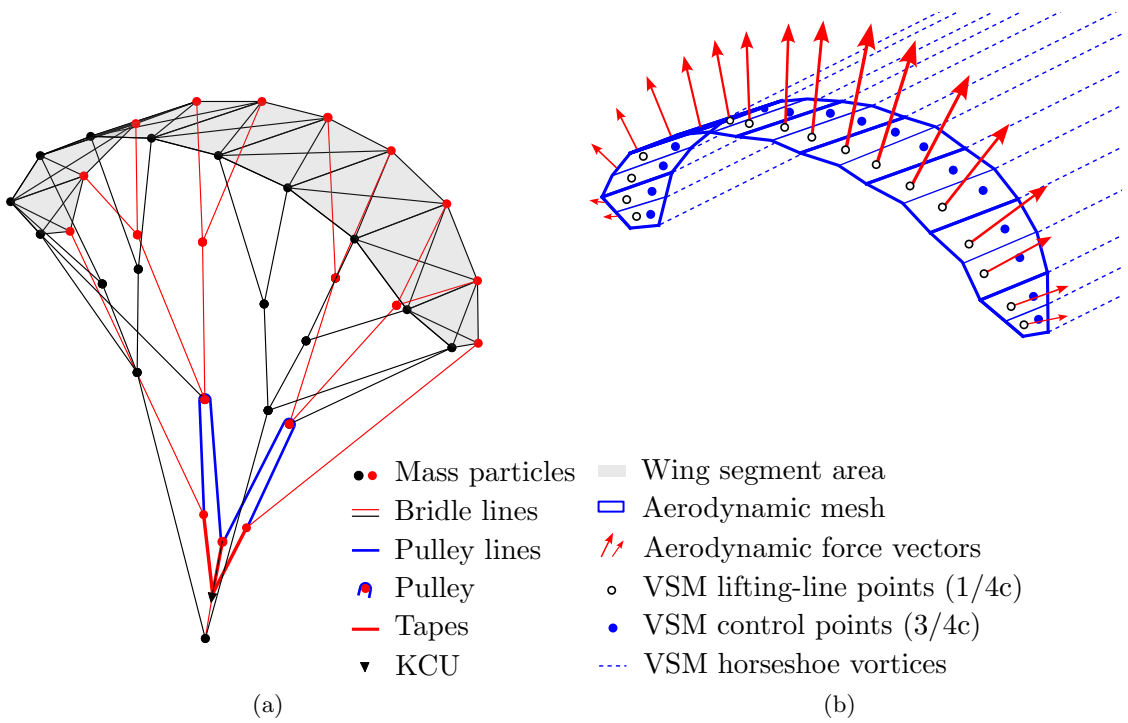

Figure 2: Aero-structural model of the V3 kite, adapted from [4]. (**a**) The kite structure is a distributed mass model coupled with spring-damper elements. The two diagonal lines per wing segment are additional spring-damper elements used as cross members to prevent shear deformation. (**b**) The VSM model of the segmented wing is depicted with two VSM panels per wing segment.

suitable due to its stability for highly nonlinear problems [6, 11]. The KDR algorithm tracks the global kinetic energy and when a peak is detected, sets all nodal velocities to zero. This is not a physical form of damping but a numerical trick that increases stability and decreases computational time. If the system is not yet in a static equilibrium the unresolved force balance will create a residual acceleration. This residual acceleration will create a velocity that will drive this system toward the static equilibrium. Resulting in pseudo-time scale steps that reach a steady-state solution without representing the physical transient phase. By comparing steady-state analytical solutions and experiments, it was verified and validated that the solver with the KDR algorithm asymptotically approaches the steady-state solution [11].

Critical for ensuring solver convergence, an initialization procedure is introduced where the inflow conditions are increased from a baseline in steps to the desired value, i.e., as if the wind would slowly build up to the desired value. The actuation input is fed into the system in steps starting from the powered design state, i.e., depower tape at its minimum length. Each steering- or depower-tape step change is only applied after the kite finds a quasi-steady equilibrium.

3. Virtual Wind Tunnel setup

The VWT simulation setup reduces an AWE system to a kite inside a box see Figure 3(a). In the symmetric condition, the box orients itself with the wind axis reference frame. To converge to a quasi-steady state, the aero-structural coupled kite simulation must find equilibrium over all six DOF. The bridle point **B** forms the connection point between the kite and tether, which has zero rotational resistance. In the VWT, a boundary condition is placed at **B**, providing zero

rotational resistance and equal and opposite forces in the tether direction, resembling the tether force.

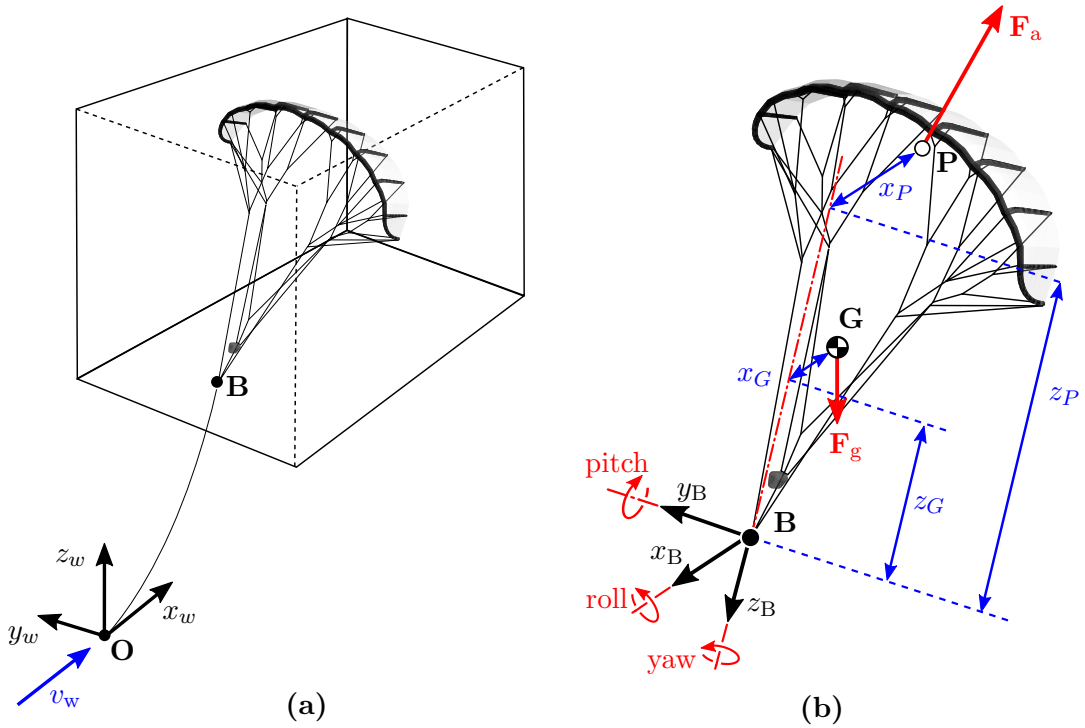

Figure 3: Soft-wing AWE system in idealized symmetric conditions. **(a)** shows the VWT box, the wind vector v_w, origin **O** and bridle point **B**. **(b)** depicts a pitched kite, the body axis reference frame, pitch, roll, yaw, aerodynamic force $\mathbf{F}_a$, gravitational force $\mathbf{F}_g$, the center of gravity **G**, the center of pressure **P**, and the distances to both these points in z_B-direction and x_B-direction.

3.1. Symmetry Assumption

In idealized conditions and straight flight parallel to the wind, one can assume the presence of a symmetry plane on the $x_w z_w$-plane for both the kite geometry and the inflow conditions. This leads to zero roll- and yaw moments and a force equilibrium in the y_w-direction. The bridle point boundary condition ensures a translation equilibrium for the non-zero kite forces in the x_w- and z_w-direction. To find a zero pitch moment around the bridle point $M_{B,\theta}$, the kite must be pitch statically stable, i.e., a counter-reacting moment must be produced when the pitch angle θ changes,

$$\frac{dM_{B,\theta}}{d\theta} < 0. \tag{4}$$

Computing the derivative of $M_{B,\theta}$ is not straightforward because each variable is non-linearly dependent on the pitch angle θ,

$$M_{B,\theta} = F_{a,x}(\theta) z_p(\theta) + F_{g,x}(\theta) z_G(\theta) - F_{a,z}(\theta) x_p(\theta) - F_{g,z}(\theta) x_G(\theta). \tag{5}$$

Experiments and previously run aero-structural coupled kite simulations [4, 8] indicate that the V3 kite is pitch statically stable, i.e. Equation (4) holds. Dynamic stability is not discussed, as the aero-structural coupled simulations are quasi-steady.

When the symmetry plane assumption does not hold due to asymmetric inflow conditions, steering actuation, roll, or other, the forces in the y_w-direction no longer cancel out, and the yaw and roll moments are not zero. Finding equilibrium for a flight condition without a symmetry plane is non-trivial as most kites, including the V3 kite, are not roll statically stable, partly attributed to the anhedral shape. In practice, the kite requires continuous steering input, and the position depicted in Figure 3(a) is an unstable equilibrium point.

3.2. Steady Circular Flight

An idealized condition called steady circular flight is considered for studying the turning behavior of the kite. With a steady uniform inflow field and an idealized kite, asymmetry is introduced through a steering input that morphs the wing, creating a non-zero aerodynamic side force that causes the kite to turn. The side force pulls the kite inwards towards the turning axis and is balanced by the inertial force that pulls the kite outwards. Gravity must be to orient the flight trajectory along the wind vector without active control input; see Figure 4. The assumption is reasonable because the operating point is in crosswind flight, where the aerodynamic forces are an order of magnitude larger than the gravitational force. In this idealized condition, the kite moves along a circular trajectory with a constant rotational velocity and constant turning radius, not requiring further control input. Due to the rotating reference frame that orients itself tangential to the circular trajectory and along the wind vector, each operating point on the circle is identical from the VWT perspective. In other words, the perpetual circular motion will appear static from the VWT perspective, indicating that a quasi-steady equilibrium over all six DOF can be found. This can only be considered a steady flight state from a rotating reference frame because the constant magnitude velocity does change direction in a fixed reference frame, i.e., the acceleration is not zero.

To explain how the kite finds an equilibrium, first, the $x_\mathrm{w}y_\mathrm{w}$-plane is considered; see Figure 4. In the depicted operating point, tether drag is in the y_w-direction ($F_\mathrm{t,y}$) and is computed as

$$F_\mathrm{t,y} = \frac{1}{8}\rho D_\mathrm{t} l_\mathrm{t} C_\mathrm{D,t} v_\mathrm{a}^2 \tag{6}$$

where ρ is the air density, D_t the diameter of the tether, l_t the length of the tether and $C_\mathrm{D,t}$ the drag-coefficient of the tether [14]. In steady-circular flight, the kite finds a constant angular velocity where the forces in the forward, the y_w-direction in Figure 4, are in equilibrium. In the simulation, this phenomenon is represented by adjusting the kite speed v_k such that the kite forces in the y_w-direction $\mathbf{F}_\mathrm{a,y}$ are equal and opposite to the tether drag, i.e.

$$\mathbf{F}_\mathrm{a,y} = -\mathbf{F}_\mathrm{t,y}. \tag{7}$$

In the x_w-direction a force equilibrium requires,

$$\mathbf{F}_\mathrm{t,x} = -\mathbf{F}_\mathrm{a,x}, \tag{8}$$

where $\mathbf{F}_\mathrm{t,x}$ represents the tether force in the x_w-direction and $\mathbf{F}_\mathrm{a,x}$ the aerodynamic force. Similar to the case where a symmetry plane can be assumed, a zero pitching moment $M_{\mathrm{B},\theta}$ is found because the kite is pitch statically stable.

Focussing on the $x_\mathrm{w}z_\mathrm{w}$-plane, see Figure 4, one finds that a force equilibrium in the z_w-direction entails,

$$\mathbf{F}_\mathrm{t,z} + \mathbf{F}_\mathrm{a,z} = -\mathbf{F}_\mathrm{c}, \tag{9}$$

where $\mathbf{F}_\mathrm{c}$ represents the centrifugal force that always orients itself in the radial direction, parallel to the z_w-axis for the presented operating point. The centrifugal force is a fictitious force that has to be included because the kite reference frame, i.e., the VWT, is rotating [15]. Due to the

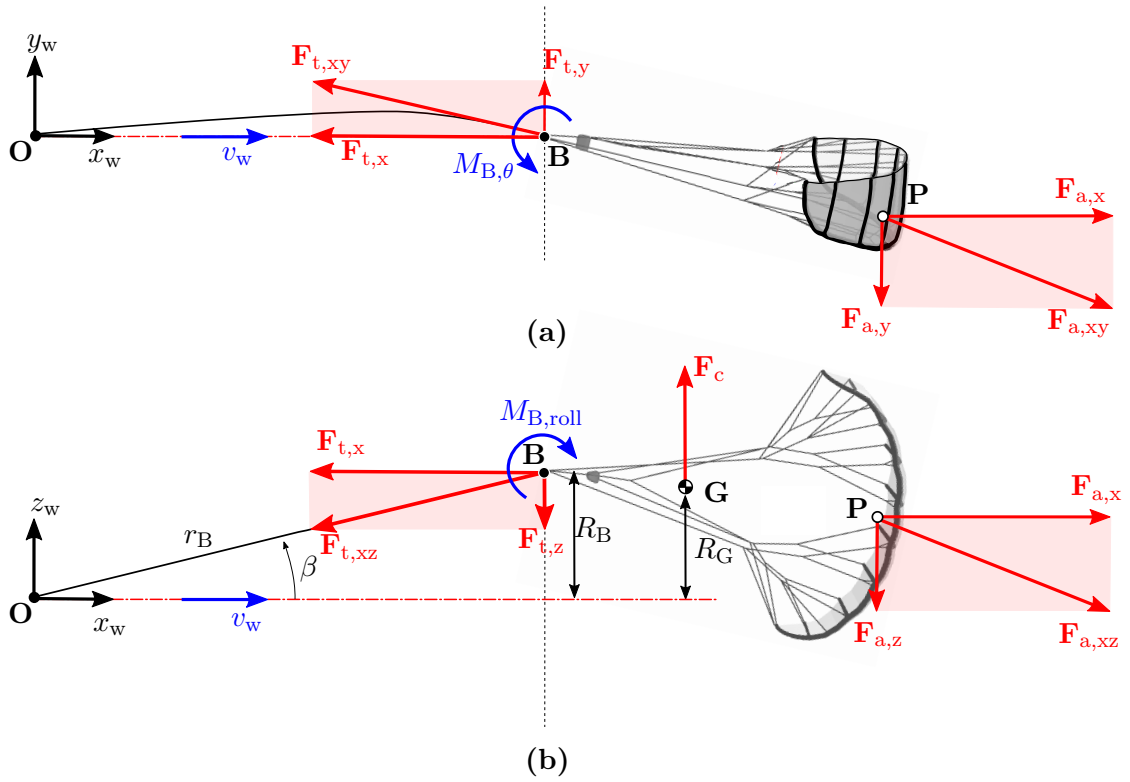

Figure 4: Steady circular flight showing the forces and moments acting on the kite. The circular trajectory is represented by the dotted line. **(a)** Depicts the $x_w y_w$-plane, similar to a classic crosswind flying kite illustration and **(b)** depicts the $x_w z_w$-plane. The tether length projection in this plane r_B, elevation angle β, the bridle point turning-axis distance R_B and the center of gravity turning-axis distance R_G are shown.

quasi-steady nature, the accelerations in each time step are assumed to be zero, and the fictitious Euler and Coriolis forces can be neglected. For neglecting the Coriolis force, the radial velocity must be zero, which can be assumed because each time step is modeled as if the converged constant radius turning motion is found.

According to Equation (9), with a zero $\mathbf{F}_{t,z}$, the aerodynamic side force $\mathbf{F}_{a,z}$ and centrifugal force $\mathbf{F}_c$ are equal in magnitude. This is problematic because with different moment arms, see Figure 4, and equal forces, one never finds a zero roll moment $M_{B,roll}$. A non-zero $\mathbf{F}_{t,z}$ is thus necessary for a zero roll moment, implying that a non-zero elevation angle β is required. The centrifugal force provides a counter-reacting roll moment that, with a non-zero $\mathbf{F}_{t,z}$, can lead to a roll statically stable kite in the steady-circular flight case.

The kite wing is backward-swept, which generally implies that it is yaw statically stable. When a wing half moves forward from a backward swept position, it will generate more lift and drag, and the latter can cause it to rotate back. The drag-induced counter-reacting yaw moment can cause yaw static stability. Furthermore, the increase in lift causes the kite to roll, indicating a yaw-roll moment coupling, which was also found for other LEI kites [16]. Not only does a yawing motion influence the rolling moment, but all rotations impact one another. Instead of deriving all nine static stability derivatives, a non-trivial exercise for a body subject to actuation-induced morphing and strong aero-structural coupling, a case-by-case methodology is adopted, and an indication of stability is found when the simulation converges.

3.3. Running the simulation

The steady-circular flight simulation is initialized by running one aero-structural coupled loop with a small steering input, resulting in non-zero aerodynamic side forces. The iterative loop starts by running the aerodynamic model. With the forces known, one can check if a force-equilibrium in the y_w-direction holds, i.e., if Equation (7) is satisfied. If that's not the case, a numerical optimization scheme adjusts the magnitude of $\mathbf{v}_\mathrm{k}$.

By neglecting the inertial and gravitational force, it is assumed that the tether projection r_B in the $x_\mathrm{w}z_\mathrm{w}$-plane is a straight line. The projected length is assumed to be 90% of the tether length. From Figure 4, one finds the following trigonometric relations,

$$\tan\beta = \frac{F_\mathrm{t,z}}{F_\mathrm{t,x}}, \tag{10}$$

$$\sin\beta = \frac{R_\mathrm{B}}{r_\mathrm{B}}, \tag{11}$$

$$F_\mathrm{t,z} = F_\mathrm{t,x}\tan\left(\arcsin\frac{R_\mathrm{B}}{r_\mathrm{B}}\right). \tag{12}$$

The distance from the center of gravity to the turning axis R_G can be found using,

$$R_\mathrm{G} = R_\mathrm{B} - d_\mathrm{BG}, \tag{13}$$

where d_BG represents the radial distance between **B** and **G**. Assuming that a force equilibrium holds over both the x_w and z_w axis, substituting Equation (8), (9) and (13) and replacing $\mathbf{F}_\mathrm{c}$ with the centrifugal force equation one finds,

$$\frac{m_\mathrm{k}v_\mathrm{k}^2}{R_\mathrm{B} - d_\mathrm{BG}} = F_\mathrm{a,x}\tan\left(\arcsin\frac{R_\mathrm{B}}{r_\mathrm{B}}\right) + F_\mathrm{a,z}. \tag{14}$$

where m_k represents the mass of the kite. Equation (14) is solved using the previous iteration value of d_BG, to find R_B, and with it, R_G is found. The kite velocity $\mathbf{v}_{\mathrm{k},i}$, apparent wind speed $\mathbf{v}_\mathrm{a,i}$ and centrifugal force $\mathbf{F}_{\mathrm{c},i}$ at each node i vary with radial distance and can be computed using

$$\mathbf{v}_{\mathrm{k},i} = \mathbf{v}_\mathrm{k}\frac{R_\mathrm{B} + R_\mathrm{BG,i}}{R_\mathrm{G}}, \tag{15}$$

$$\mathbf{v}_\mathrm{a,i} = \mathbf{v}_\mathrm{w} - \mathbf{v}_{\mathrm{k},i}, \tag{16}$$

$$\mathbf{F}_{\mathrm{c},i} = \frac{m_i v_{\mathrm{k},i}\mathbf{v}_{\mathrm{k},i}}{R_\mathrm{B} + R_\mathrm{BG,i}}, \tag{17}$$

where $R_\mathrm{BG,i}$ represents the radial distance from node i to **B**, and m_i the nodal mass. With the distribution of the external forces, the structural model computes the displacements and internal forces. The last step checks convergence and a new iteration begins if it is not found.

4. Results

The undeformed and deformed shapes are shown in Figure 5, from which one concludes that the kite has rolled to the side due to the steering tape actuation. For the given 5 cm of steering tape offset, the kite produces a side force $F_\mathrm{a,z}$ of 560 N, roughly 10% of the lift. The $F_\mathrm{a,z}$ induced roll-moment is balanced by the centrifugal force induced roll-moment at a turning radius of 19.6 m. To find the steady circular flight state, the kite accelerated from an initial v_k of 20 m/s to a final constant tangential velocity of 24 m/s. The settings used to model the V3 kite in a steady circular flight are shown in Table 1. The stiffness is taken at a lower than physical value, and the effect on the steady-state solution is minimized by ensuring the maximum elongation of the spring-damper elements is below 1% [4].

Table 1: Simulation settings

Property	**Value**	**Property**	**Value**
Wind speed v_w	4 m/s	Wing, KCU, Bridle -mass	11, 8.4, 3.4kg
Tether length l_t	200 m	Depower tape; initial-final	1.098-1.108m
Tether diameter D_t	0.04 m	Right steering tape; initial-final	1.601-1.651m
KCU equivalent diameter D_{eq}	0.38 m	KCU drag coefficient	0.47
Bridle normal drag C_τ	1.1 [6]	Stiffness	4×10^4 N/m
Bridle shear drag C_f	0.02 [6]	Time step	0.01 s

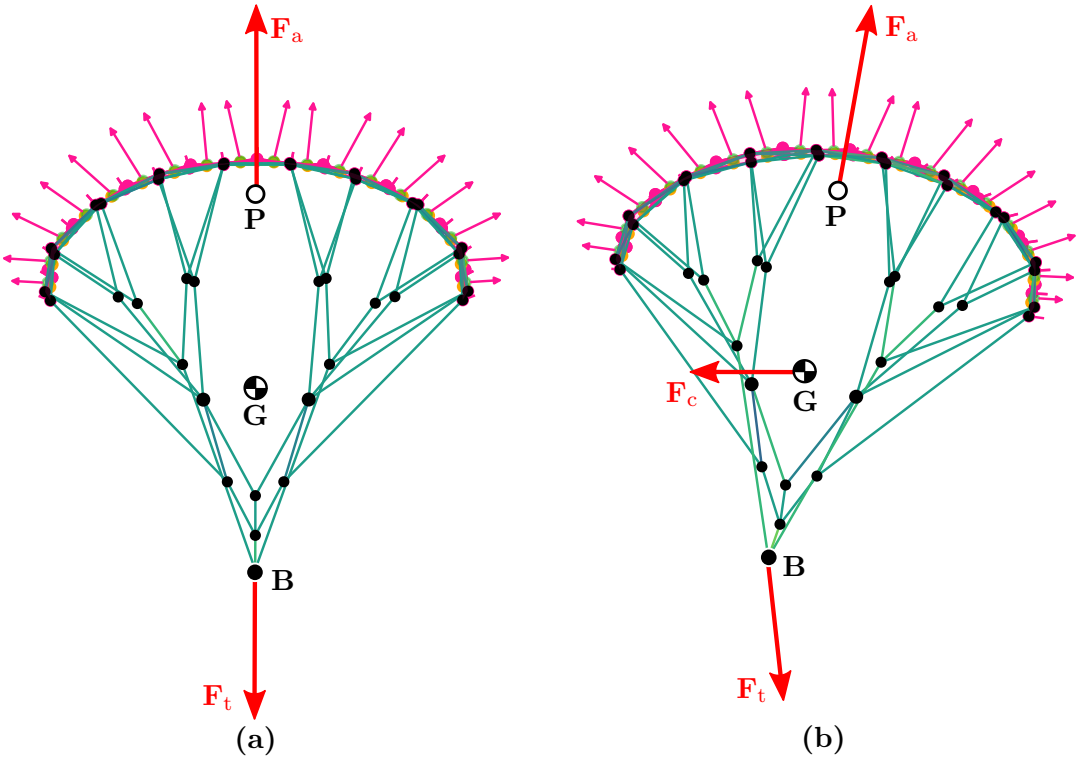

Figure 5: Frontviews of the simulation results, including resultant force vectors added in post-processing and not to scale. **(a)** Shows the resulting kite after a simulation with a symmetric assumption, and **(b)** shows the results from a steady circular flight simulation.

5. Conclusions and Discussion

This paper presents a novel methodology for quasi-steady simulations of asymmetrically deforming soft-wing airborne wind energy kites with suspended control units. First, an aero-structural model was presented with several improvements: an aerodynamic bridle line model, non-uniform mass distribution, object-oriented programming architecture, a kinetic dynamic relaxation algorithm, and an initialization procedure. Quasi-steady virtual wind tunnel simulations are performed by assuming the presence of a symmetry plane. The symmetry plane ensures a roll and yaw moment equilibrium, leaving only the pitch rotational degree of freedom. A static equilibrium is often found since most soft-wing kites are pitch-statically stable. The assumption of symmetry is required for a static equilibrium to exist. Because quasi-steady simulations do not converge without a static equilibrium, this restricts the analysis to flight

conditions for which the symmetric assumption holds.

A novelty of this paper is the introduction of the idealized steady circular flight state in which a quasi-steady equilibrium can be found without a symmetric assumption. By neglecting gravity, the kite flies in a perpetual circular turning motion around the wind vector with a constant radius and rotational velocity without active control input. As the virtual wind tunnel reference frame rotates with the kite, a fictitious centrifugal force must be included. When modeling an idealized condition with a wind-aligned tether, a force equilibrium in the radial direction requires both aerodynamic side and centrifugal force to be equal in magnitude. Because these forces act at different locations, i.e., have different moment-arms, one cannot find both a force- and moment equilibrium. This is resolved by including an elevation angle, which introduces a radial tether force component that acts at the bridle point. With this contribution, the centrifugal force can balance the aerodynamic side force-induced roll moment, causing a roll statically stable condition that leads to a static equilibrium. Within the aero-structural coupled simulation loop, the turning radius is computed to find the velocity- and centrifugal force distributions, varying with radial distance. With radial distance and steering setting, one can derive the first simulated turning laws without relying on empirical data.

Future work should use multiple simulations to find turning relations and validate these with empirical turning laws. Validation by comparing experimental data will require modeling a realistic flight pattern, possibly done by coupling to a dynamic model. A tether sag model and an aerodynamic post-stall correction model should be included. Because the current aerodynamic model implementation can result in a saw-tooth spanwise lift distribution, a correction is needed and anticipated to increase the accuracy and robustness of the simulation.

Funding: This work is part of the NEON research program and received funding from the Dutch Research Council NWO under Grant Agreement No. 17628 and co-funding from Kitepower B.V. The APC was covered by Delft University of Technology.

Conflicts of interest: Both authors are full-time employees of Delft University of Technology. R.S. is a co-founder of Kitepower B.V.

References

[1] Van Hagen L, Petrick K, Wilhelm S and Schmehl R 2023 *Energies* **16** 1750
[2] Kleidon A 2021 *Meteorologische Zeitschrift* **30** 203–225
[3] Breukels J 2011 *An Engineering Methodology for Kite Design* Ph.D. thesis Delft University of Technology
[4] Poland J A W and Schmehl R 2023 *Energies* **16** 5264
[5] Kitepower airborne wind energy - plug & play, mobile wind energy URL `https://thekitepower.com/`
[6] Thedens P 2022 *An integrated aero-structural model for ram-air kite simulations: with application to airborne wind energy* Ph.D. thesis Delft University of Technology
[7] Vermillion C, Cobb M, Fagiano L, Leuthold R, Diehl M, Smith R S, Wood T A, Rapp S, Schmehl R, Olinger D and Demetriou M 2021 *Annual Reviews in Control* **52** 330–357
[8] Cayon O, Gaunaa M and Schmehl R 2023 *Energies* **16** 3061
[9] Hoerner S F 1965 *Fluid-dynamic drag* (Hoerner fluid dynamics)
[10] Geschiere N H 2014 *Dynamic modelling of a flexible kite for power generation: Coupling a fluid-structure solver to a dynamic particle system* Master's thesis Delft University of Technology
[11] Batchelor A R 2023 *Development and benchmarking of a Particle System framework for structural modeling of soft-wing kites* Master's thesis Delft University of Technology
[12] van der Vorst H A 1992 *SIAM Journal on Scientific and Statistical Computing* **13** 631–644
[13] Day A 1965 *The Engineer* **219** 218–221
[14] Argatov I and Silvennoinen R 2013 Efficiency of traction power conversion based on crosswind motion *Airborne Wind Energy* Green Energy and Technology ed Ahrens U, Diehl M and Schmehl R (Springer) chap 4, p Chapter 4
[15] Arnold V I 1989 *Mathematical Methods of Classical Mechanics* 2nd ed (Springer)
[16] Terink E J 2009 *Kiteplane Flight Dynamics: Stability and control analysis of tethered flight for power generation purposes* Master's thesis Delft University of Technology